Scientific Research Publishing

World Journal of Mechanics, 2023, 13, 1-19
https://www.scirp.org/journal/wjm
ISSN Online: 2160-0503
ISSN Print: 2160-049X

Flow Dynamics around Two Side by Side Circular Cylinders with Alternating Movements

Alice Rosa da Silva

Faculty of Civil Engineering, Federal University of Uberlandia, Uberlandia-MG, Brazil
Email: alicers@ufu.br

How to cite this paper: da Silva, A.R. (2023) Flow Dynamics around Two Side by Side Circular Cylinders with Alternating Movements. *World Journal of Mechanics*, **13**, 1-19.
https://doi.org/10.4236/wjm.2023.131001

Received: November 7, 2022
Accepted: January 9, 2023
Published: January 12, 2023

Abstract

The flow dynamics is analyzed through two-dimensional numerical simulations around two circular cylinders arranged side by side, with 4 combinations of alternating motions. All simulations are performed for Re = 1000, amplitude of oscillation (A) equal to 3, frequency ratio (f_r) of 0.5, specific rotation (a) equal to 0.5 and different values of spacing ratio (L/D). It is verified that the combination of the type of movement, together with the position of one cylinder in relation to the other, exerts significant influence on the flow dynamics, as well as on the pressure distribution around the cylinder surface and on the average values of the fluid dynamics coefficients. The smallest value of the average pressure coefficient ($C_p = -3.3$), is obtained for the oscillating cylinder when placed side by side with the clockwise rotation cylinder, case 3 and $L/D = 1.5$. On the other hand, the lowest mean drag coefficient ($C_d = 1.0788$), is obtained for the cylinder with counterclockwise rotation, located in the lower position in relation to oscillating cylinder in the upper position, with spacing between them of 1.5. Furthermore, it is observed that the rotation movement is more effective in reducing drag than the rotation-oscillation movement, for the studied frequency ratio.

Keywords

Rotation, Rotation-Oscillation, Flow Dynamic, Circular Cylinder

1. Introduction

Fluid dynamics is an area that has been studied for several decades. Due to its technological relevance and the wide range of interesting mathematical problems, it remains one of the most important areas for engineering. And, although the study of incompressible flows around bluff bodies is one of the oldest problems in fluid mechanics, it is still today one of the most important and challeng-

ing. According to [1], such flows can result in phenomena, which help in understanding the physics of biological propulsion, in the interaction of wind and sea waves with offshore structures, and vortex-induced vibrations for better flow control.

Thus, cylindrical structures immersed in the transverse flow such as in heat exchanger projects, nuclear reactor fuel rods, steel cables of suspension bridges, among others [2], flows around structures such as tall buildings, submarine periscopes, and industrial devices like cooling towers [3] are of the great interest in practice. Also, flow around circular cylinders [4] [5] [6] [7], as well as flow around rectangular cylinder [8], has been studied by different researchers, considering several aspects, in order to investigate the mechanisms behind these phenomena. According to [9], flow induced vibration, FIV, of the elastic bodies are not rare. They occur in a wide variety of physical systems, such as airplane wings, leaves of trees, bridges of long span, tall buildings, clarinet reeds or offshore structures to name a few. Vortex-induced vibration, VIV, is a type of FIV caused by the phenomenon of non-linear resonance. Due to the relevance of the subject, following this line of research, other scholars [6] [10] [11] [12], have also contributed to investigations with similar studies.

On the other hand, flow around a group of cylinders, such as risers of offshore platforms, has been a challenge due to its inherent complexity. The interference between cylinders is responsible for several significant changes in flow characteristics. According [13], such structures are subject to shear and oscillatory flows and, therefore, can experience flow-induced vibration, which could lead to structural failure or shutdown of industrial facilities under certain conditions. Therefore, it is worth studying such problems, to better understand the wake behavior when multiple cylinders are placed in a fluid stream. According [7], the motions induced by vortex can not only impact the mooring and riser systems, but also may cause collision between the floating structure and the nearby supporting vessels. Consequently, vortex-induced motion became a critical problem during the design and optimization of floating structures with multiple columns.

In view of the above, is reinforced the great relevance of vortex shedding phenomenon, in several practical situations. So, among the different objectives of researchers regarding the study of flow around bluff bodies or slender, has been the search for the suppression of this mechanism. Chehreh and Javadi [14], simulated a circular cylinder with attached swinging thin splitter plates as a passive method and analyzed the effect on the drag and lift forces, flow patterns and frequencies of vortex shedding. Another passive control method that has been explored is rotation and rotation-oscillation. Zheng and Wang [15] numerically investigated the oscillation of a two-dimensional circular cylinder attached with a short fairing device. They analyzed the mechanism behind the galloping oscillation of the fairing device combining the cylinders movements and the corresponding vorticity fields. Ping *et al.* [16] performed two-dimensional high-order spectral/hp simulations for a cylinder undergoing a sinusoidal rotary oscillation about its own axis. They further used the proper orthogonal decomposition

(POD) to characterize the spatially evolving nature of the forced wake as it undergoes a transition from the near-wake two-layer shedding pattern to the far-wake Kármán-like shedding pattern. In the study [1] about three-dimensional turbulent flow around a circular cylinder with sinusoidal rotation oscillation movement, they verified that under forced control, 50% of drag reduction is obtained and the three-dimensionality of the flow is reduced in the lock-on regime. Effects of the oscillation and rotation of the cylinder on the vortex shedding in lock-on and non-lock-on regions, the mean drag and lift coefficients and the Strouhal number are investigated in detail [2]. Different flow patterns are observed and classified [14]. They verified that in certain configurations, an in-phase vortex shedding pattern is dominant and the oscillatory nature of the lift force completely disappears. Given the relevance of the exposed subjects, the present work aims to contribute with one of the passive control methods, already mentioned. The combination of the rotation effect of one cylinder with the rotation-oscillation effect of another cylinder, not yet investigated, is presented in this work. The combined effect of these movements is analyzed through the flow dynamics, as well as the relevant parameters such as the fluid dynamic coefficients and the pressure distribution around the cylinder surface. Different spacing ratios between the cylinders, for equals oscillation amplitude, frequency ratio and specific rotation are considered in the simulations. The Immersed Boundary (IB) method [17], widely used by several researchers [4] [6] [13] [18] [19] [20] due to many advantages, such as ease of implementation, flow study on simple, complex and even deformable geometries without the need of remeshing, is also used in this study.

This paper is divided in 5 items, which are: introduction, mathematical and numerical method, problem description, results and conclusions. In the introduction, relevant works involving fluid dynamics, in the study of flow over moving bodies and works dealing with the methodology used in the present work are presented. In item 2, the mathematical formulation that involves the IB methodology, the numerical method and turbulence modeling are succinctly presented. In item 3, a description of the problem is made for the simulations with two circular cylinders with different movements. In item 4, the results and discussions of the simulations with imposed motion—rotation and rotation-oscillation—are presented. In the item 5, the conclusions are presented, as well as the perspectives for future work. Finally, is presented the consulted bibliographic references.

2. Mathematical and Numerical Method

2.1. Basic Equations

In the IB methodology, the governing equations for two-dimensional, viscous, incompressible and Newtonian flow are given by:

$$\frac{\partial u_i}{\partial t}+\frac{\partial\left(u_i u_j\right)}{\partial x_j}=-\frac{1}{\rho}\frac{\partial p}{\partial x_i}+\frac{\partial}{\partial x_j}\left[\nu\left(\frac{\partial u_i}{\partial x_j}+\frac{\partial u_j}{\partial x_i}\right)\right]+f_i. \quad (1)$$

$$\frac{\partial u_i}{\partial x_i} = 0. \tag{2}$$

where ρ [Kg/m^3] and ν [m^2/s] are the specific mass and the kinematic viscosity, respectively. The other variables u_i [m/s], p [N/m^2], f_i [N/m^3] are respectively, the *i-th* component of the velocity, the pressure and the *i-th* Eulerian force component. The last term of Equation (1) is obtained by the distribution of the components of the Lagrangian interfacial force vector, $\boldsymbol{F}(\boldsymbol{x}_k,t)$ [N], by Equation (3), using a distribution function [21].

$$\boldsymbol{f}(\boldsymbol{x},t) = \sum_k D_{ij}(\boldsymbol{x}-\boldsymbol{x}_k)\boldsymbol{F}(\boldsymbol{x}_k,t)\Delta S^2(\boldsymbol{x}_k). \tag{3}$$

Being $\boldsymbol{f}(\boldsymbol{x},t)$ [N] the Eulerian force vector; $\boldsymbol{x}$ [m] and $\boldsymbol{x}_k$ [m], the position vectors of the Eulerian and Lagrangian points, respectively; ΔS [m] the average length of the arc over the Lagrangian points and D_{ij} [m^{-2}] an interpolation/distribution function, with properties of a Gaussian function. The $\boldsymbol{F}(\boldsymbol{x}_k,t)$ term [22] is given by Equation (4) and the Gaussian function by Equation (5):

$$\boldsymbol{F}(\boldsymbol{x}_k,t) = \boldsymbol{F}_a(\boldsymbol{x}_k,t) + \boldsymbol{F}_i(\boldsymbol{x}_k,t) + \boldsymbol{F}_v(\boldsymbol{x}_k,t) + \boldsymbol{F}_p(\boldsymbol{x}_k,t). \tag{4}$$

$$D_{ij}(\boldsymbol{x}-\boldsymbol{x}_k) = \frac{g\left[(x_k-x_i)/h\right]g\left[(y_k-y_j)/h\right]}{h^2}. \tag{5}$$

with $g(r) = g_1(r)$ if $\|r\| \le 1$, $g(r) = \frac{1}{2} - g_1(2-\|r\|)$ if $1 < \|r\| < 2$, $g(r) = 0$ if $\|r\| \ge 2$ and $g_1(r) = \left(3 - 2\|r\| + \sqrt{1+4\|r\|-4\|r\|^2}\right)/8$.

In Equation (4) $\boldsymbol{F}_a$ [N] is the acceleration force, $\boldsymbol{F}_i$ [N] the inertial force, $\boldsymbol{F}_v$ [N] the viscous force and $\boldsymbol{F}_p$ [N] the pressure force. The first represents the portion of the greatest influence on the total Lagrangian force calculation, can be interpreted as the portion that guarantees the non-slip condition. And, in Equation (5) r is the radius of influence of the distribution function which can be $(x_k - x_i)/h$ or $(y_k - y_j)/h$ depending on the direction in which the property is distributed, h is the size of the Eulerian mesh and (x_i, y_j) are the coordinates of the Eulerian points.

For the numerical method, the Fractional Step method [23] is used with shifted meshes for the coupling between the pressure and velocity fields. It is a non-iterative method of pressure correction, where from the force, velocity and the pressure fields of the previous iteration, an initial velocity field is estimated. With these estimated velocity fields, the pressure correction field is calculated, through the solution of a linear system by the Modified Strongly Implicit procedure (MSI) [24]. Then, the new velocity field is obtained, which satisfies the continuity equation. Only one iteration, in each time step, is necessary for the velocity fields obtained to satisfy the continuity, according to the established criterion, which in the present work is 1.0E-5 as maximum mass residue over all cells of the domain.

The spatial discretization is performed using the second-order centered finite difference scheme and the temporal discretization with the first-order Euler method, Equation (6), and second-order Adams-Bashforth, Equation (7), as follow:

$$\frac{\tilde{u}_i^{n+1}-u_i^n}{\Delta t}=g\left(u_i^n,u_j^n\right)-P_i^n+F_i^n. \tag{6}$$

$$\frac{\tilde{u}_i^{n+1}-u_i^n}{\Delta t}=\frac{3}{2}g\left(u_i^n,u_j^n\right)-\frac{1}{2}g\left(u_i^{n-1},u_j^{n-1}\right)-P_i^n+F_i^n. \tag{7}$$

where $\tilde{u}$ is the estimated velocity, Δt is the time step, g corresponds to the advective and diffusive terms of the motion equation, P_i^n is the pressure gradient and F_i^n the force field.

2.2. Equations for Turbulence

In our daily, there are many opportunities to observe turbulent flows, such as smoke from a chimney, water from a river or waterfall, or the buffeting of a strong wind. In these observations, we immediately see that the flow is unsteady, irregular, apparently random and chaotic, and certainly the motion of every eddy or droplet is unpredictable [25]. The flow around bluff body, in this case a circular cylinder, even at moderate Reynolds number causes the generation and shedding of vortices. And, being the spatial discretization scheme, centered and without numerical diffusion, it is natural that the calculations from the simulations become unstable. Hence the need to use of the turbulence model to ensure that the kinetic energy of the turbulence is carried by wave number or cutoff frequency. Furthermore, it is known that even for flows at moderate Reynolds number, it is not possible to directly solve all frequencies in turbulent flow. Thus, after applying the filtering and decomposition process [26] [27], and applying the definitions in Equations (1) and (2), the following equation is obtained:

$$\frac{\partial\overline{u}_i}{\partial t}+\frac{\partial\left(\overline{u}_i\overline{u}_j\right)}{\partial x_j}=-\frac{1}{\rho}\frac{\partial p^*}{\partial x_i}+\frac{\partial}{\partial x_j}\left[\nu_{ef}\left(\frac{\partial\overline{u}_i}{\partial x_j}+\frac{\partial\overline{u}_j}{\partial x_i}\right)\right]+f_i. \tag{8}$$

where $p^*=\overline{p}+2/3\rho k$ and $\nu_{ef}=\nu+\nu_t$ being ν_{ef} the effective viscosity and ν_t the turbulent viscosity given by $\nu_t=\left(C_s\ell\right)^2\sqrt{2\overline{S}_{ij}\overline{S}_{ij}}$, where ℓ is the characteristic length, S_{ij} the strain rate and C_s the Smagorinsky constant equal 0.18.

3. Problem Description

In this work, the IB methodology is used to simulate two-dimensional incompressible, isothermal and Newtonian flow around two moving circular cylinders arranged side by side. In **Figure 1(a)** the two cylinders represent the Lagrangian mesh and the calculation domain represents the Eulerian mesh. The location of the cylinders in relation to the input and output of the calculation domain is also schematized in the same figure.

Figure 1(b) shows the uniform mesh region, that contains both cylinders, as well as their distance from the limits. The finer mesh in regions with high gradients,

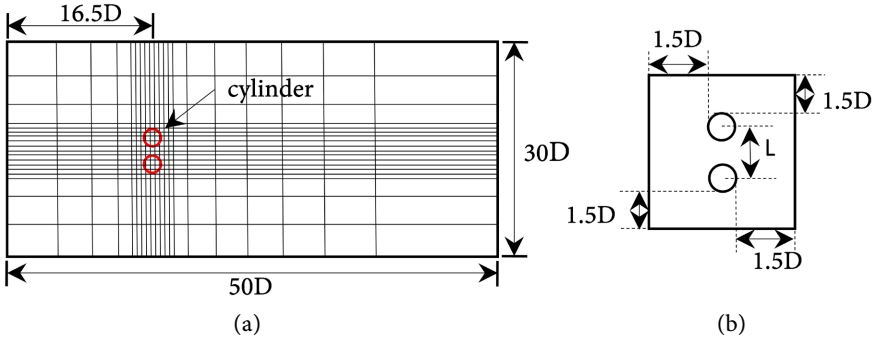

Figure 1. Illustrative scheme: (a) of the Eulerian and Lagrangian meshes; (b) distance from the cylinders surfaces to the limits of the uniform region.

close to the cylinder captures the fields better, while for regions with low gradients a coarser mesh is used. The use of a uniform mesh across calculation domain increases the computational cost unnecessarily.

For the rotation-oscillation cylinder, the tangential velocity over the cylinder is given by:

$$V_{tg} = \omega R = A\sin\left(2\pi f_c t\right) R\,. \tag{9}$$

where A [m] is the oscillation amplitude, R [m] is the radius of the cylinder, f_c [Hz] is the oscillation frequency of the cylinder or imposed frequency and t [s] is the physical time. This procedure is the same [28] and similar [1].

For the rotating cylinder, the positions of the Lagrangian points that make up the fluid-solid interface can be recalculated, according to the imposed angular velocity. Simulations can also be performed without recalculating the positions of the Lagrangian points. In this case, the rotation movement, clockwise (CR) or counterclockwise (CCR), is performed only with the projection of the tangential velocity, obtained through the imposed angular velocity, in the x and y components of the velocity, in each Lagrangian point, as shown in **Figure 2**.

For all simulations, the non-uniform grid of 600 × 300 points is used and the Reynolds number equal to 1000. The other important parameters are: oscillation amplitude (A) equal to 3 and frequency ratio ($f_r = f_c / f_o$) equal to 0.5 for the rotation-oscillation cylinder, being f_o the vortex shedding frequency for the stationary cylinder. For the rotating cylinder, the specific rotation (α) is 0.5.

And the relationship between the tangential velocity (V_t) of the cylinder and the free stream velocity, U_∞ [m/s], is given by the specific rotation parameter $\alpha = \left(\omega R\right)/U_\infty$.

Table 1 shows the types of cylinder movement, upper (cylinder 1) and lower (cylinder 0), considering the 4 simulated cases.

4. Results and Discussions

The vortex shedding phenomenon is of great importance in several practical situations, as already mentioned. Considering that many existing structures are subject to movements, results of two-dimensional numerical simulations of the

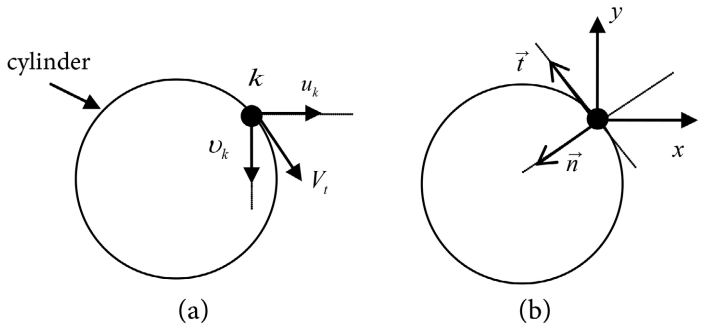

Figure 2. Illustrative scheme of the tangential velocity projection and tangential and normal vectors, respectively.

Table 1. Types of movement of each cylinder, for the 4 analyzed cases.

		Movement type	
Case 1	Cylinder 1	Rotation-oscillation (RO)	1
	Cylinder 0	Clockwise rotation (CR)	0
Case 2	Cylinder 1	Rotation-oscillation	1
	Cylinder 0	Counterclockwise rotation (CCR)	0
Case 3	Cylinder 1	Clockwise rotation	1
	Cylinder 0	Rotation-oscillation	0
Case 4	Cylinder 1	Counterclockwise rotation	1
	Cylinder 0	Rotation-oscillation	0

combination of two types of movement, rotation and rotation-oscillation, are presented in this section. The combined effect of these movements is analyzed through the behavior of the flow dynamic (vorticity fields), the fluid dynamics coefficients and the pressure distribution around the cylinders.

4.1. Vorticity Fields

The vorticity fields, after established the flow regime, are shown from **Figure 3(a)** to **Figure 3(d)**, for different spacing ratios (L/D) and two types of movements, as shown in **Table 1**. The lines correspond to the spacing ratios and the columns correspond to the 1st, 2nd, 3rd and 4th simulated cases, respectively from left to right.

For $L/D = 1.2$ (**Figure 3(a)**), case 1, there is only one wake downstream of the two cylinders, after the flow regime has been established. The vortices are rounded, large and the cylinders behave as one. There is a 2S vortex shedding mode. For cases 2 and 3, the combination of movements produces a more symmetrical wake, while combinations 1 and 4 despite producing similar wakes, the longitudinal and transverse spacings are much larger than those obtained with

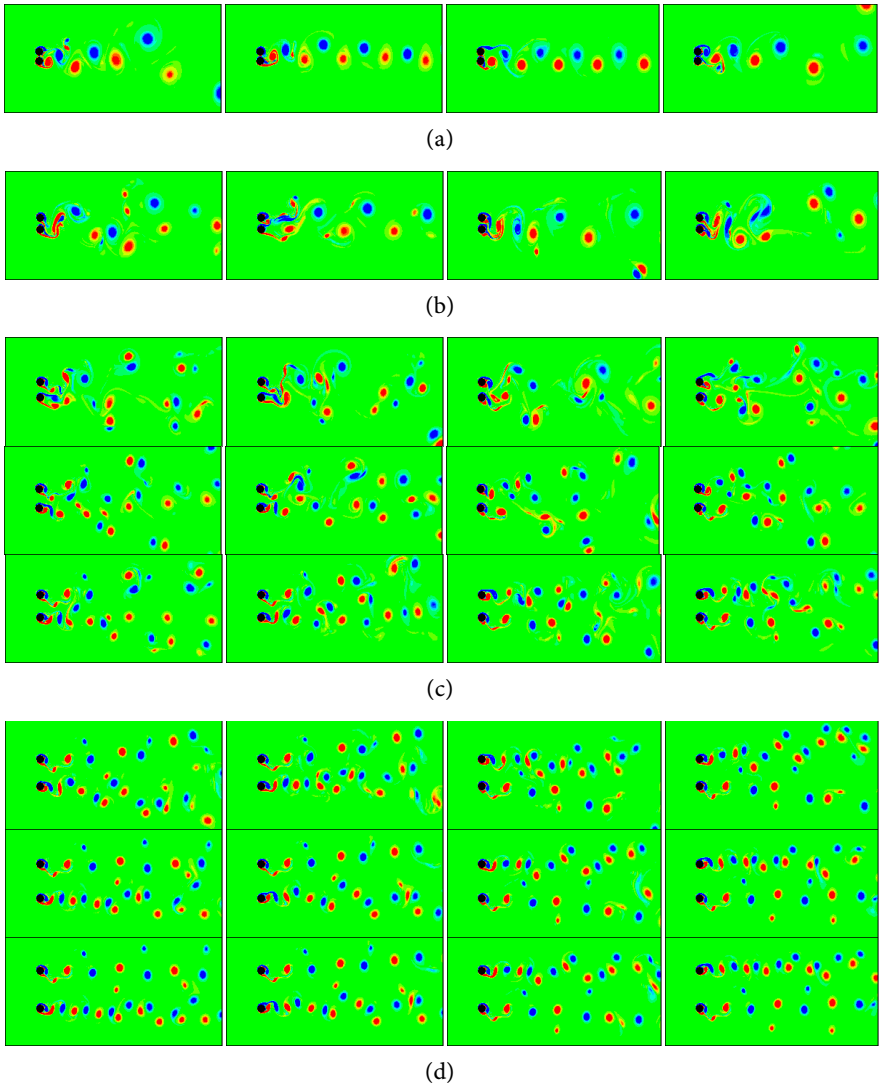

Figure 3. (a) Vorticity fields. $L/D = 1.2$ – cases 1, 2, 3 and 4 respectively. (b) $L/D = 1.5$. (c) $L/D = 2.0$, 2.5 and 3.0 respectively (top to bottom). (d) $L/D = 3.5$, 4.5 and 5.0 respectively (top to bottom).

the combinations 2 and 3. Thus, it is clear that even keeping the same spacing ratio, the combination of movements interferes in the vortex shedding process. This interference is well evident when analyzing the evolution of the vortex shedding process for the initial times of simulation as shown in Figure 4.

As the spacing ratio increases (Figure 3(b)), it is observed that the shear layers coming from the cylinders collide and, after the establishment of the stable flow regime, pairs of vortices of opposite signs are scattered in the wake (case 1). Changing the rotation direction of cylinder 0, from clockwise to counterclockwise, the shear layers coming from it suppress those originated by cylinder 1. It is noted downstream, that the transverse distance between the two shear layers of the lower cylinder is large, with a collision between the vortex generated by the upper shear layer of cylinder 0 and the vortex generated by the lower shear layer of cylinder 1. Far from the cylinders, there is only a single wake with large

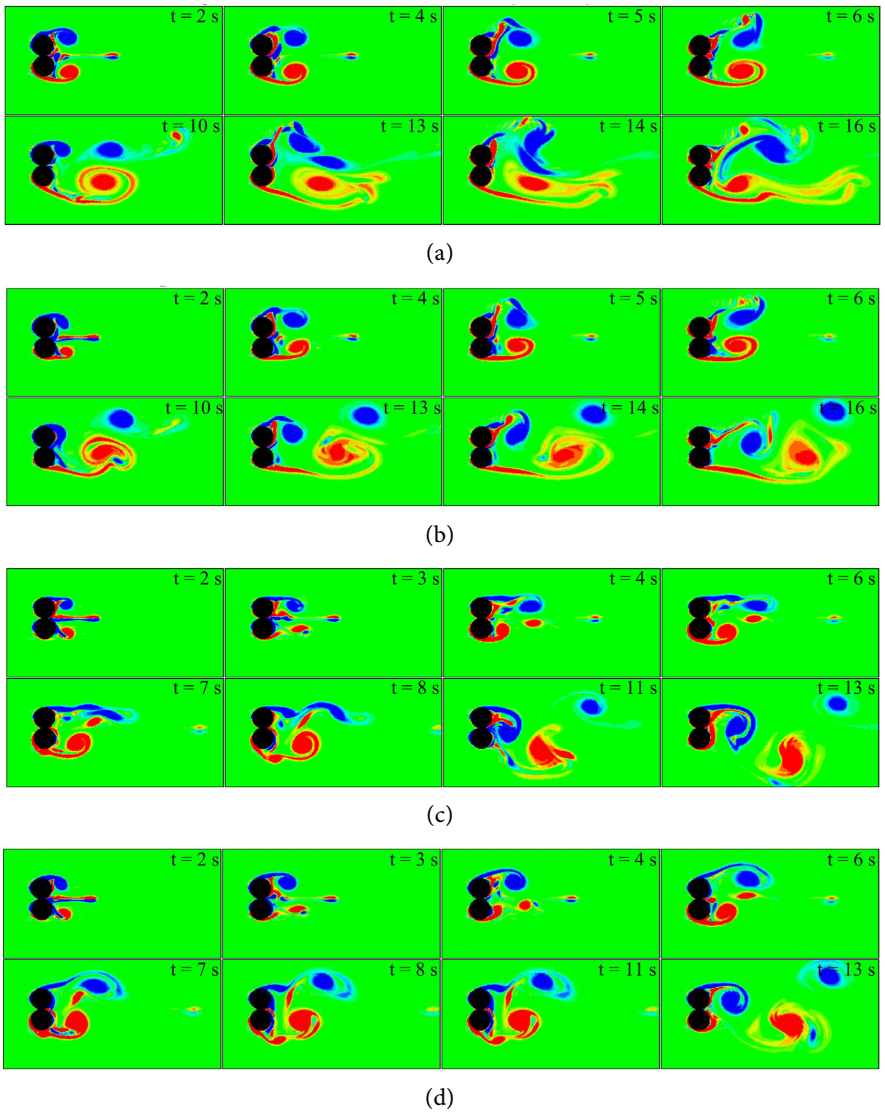

Figure 4. Evolution of the vortex shedding process for $t < 20$ s and $L/D = 1.2$. (a) Case 1. (b) Case 2. (c) Case 3 and (d) Case 4.

transverse and longitudinal spacing between the vortices, beyond to presenting a certain symmetry. With the change of movements, cylinder 0 with rotation-oscillation and cylinder 1 with clockwise rotation (case 3), the obtained wake is similar to that of case 2, when far from the cylinders. Close to the cylinders there is no distance between the shear layers of cylinder 1, with rotation, due to the fact that the rotation is clockwise. Cylinder 1, once with counterclockwise rotation, case 4, the wake loses the symmetry observed for cases 2 and 3 and, in addition, the fusion between vortices of the same sign is observed.

For $L/D \geq 2.0$ (**Figure 3(c)**), the vortex shedding process by the two cylinders becomes independent, *i.e.*, positive and negative vortices are formed by the two cylinders, regardless of the motion type. As the spacing between the cylinders increases, the amount of generated vortices also increases. It is also verified that the alternation in the type of movement, in combination with the position of one

cylinder in relation to another, influences in the vortex shedding time, even that the resulting wake after establishing the stable flow regime be similar. It is also worth to point out, that during the evolution in the vortex shedding process, occurs change in the format of the released vortices, and it may even stay as if were just a filament, beyond to the possibility of fusion between the vortices or not.

For spacing ratio $L/D \geq 3.5$ (**Figure 3(d)**), it is noted the 2C mode of vortex shedding, for the rotation-oscillation cylinder when in the upper position (cases 1 and 2) and when in the lower position (cases 3 and 4). This mode, composed by vortices pairs of the same sign, was also observed [29]. On the other hand, the wake formed by the vortices released from the rotating cylinder has the appearance of "quotes".

Figure 4(a) shows the evolution of the vortex shedding process for a simulation time of less than 20 s, case 1, $L/D = 1.2$. It can be noted for the time of 2 s that the lower shear layer of the upper cylinder and the upper shear layer of the lower cylinder are repressed due to clockwise rotation (cylinder 0) and rotation-oscillation (cylinder 1) movements, forming two vortices of small scale. Also, cylinder 1 generates a negative vortex and cylinder 0 a positive vortex, both of large scale. As the time passes, it is observed that the positive vortex will growing and stretching while a second negative vortex is generated and released from cylinder 1, which will merge with the first negative vortex released, forming only one. In this way, the process will continue over time and the wake will be formed by negative vortices originated from the upper shear layer of cylinder 1 and by positive vortices originated from the lower shear layer of cylinder 0.

The evolution of the vortex shedding process for case 2, in the first 20 s of the simulation is shown in **Figure 4(b)**. In the first 6 s, the process is similar to the case 1. It is observed that the first negative vortex is released after 4s, while the first positive vortex is only released after 16 s. Due to the fact that cylinder 0 in this case rotates counterclockwise, it is noted that, unlike what happens in case 1, the second negative vortex released after 13 s does not merge with the first. This process continues and new vortices are formed, to compose the wake over time.

For case 3, **Figure 4(c)**, where cylinder 0 has rotation-oscillation movement and cylinder 1 clockwise rotation, the first positive vortex is released after 2 s and the first negative vortex after 3 s. The negative vortex becomes elongated and merges with another elongated vortex, forming only one after 8s. In the time of 4s, a second positive vortex is formed, and, as it develops still attached to the cylinder, another positive vortex, of smaller scale, is formed, for after the time of 9 s they merge.

Thus, it is noted that after 12 s of simulations there is only a pair of vortices in the wake. Others are formed and released and the process continues.

In **Figure 4(d)**, corresponding to case 4 and $L/D = 1.2$, cylinder 1 rotates counterclockwise while cylinder 0's motion is the same as in case 3. The vortex shedding process is similar to that of case 3 in the first 6 s, but the negative vor-

tices are more rounded. It is noted with the inversion in the direction of movement of cylinder 1 that the union of the second positive vortex with the first positive of smaller scale, occurs after 11 s from the start of the simulation, while for case 3 it occurred for a lower time.

It can be said, therefore, that although the vortex wake looks similar in all cases, Figure 3(a), the alternation of movements between the cylinders, alters the time in which the vortices are generated and released from the cylinder, as shown Figure 4(a) to Figure 4(d). It is verified that the first vortex is released in a shorter simulation time, when the lower cylinder has rotation-oscillation movement. It is also noted, for the spacing ratio equal to 1.2, that the cylinders movement prevents the formation and shedding of large-scale vortices from the lower and upper shear layers, of cylinders 1 and 0 respectively.

Next, the influence of alternating movements on the pressure distribution around the cylinders is analyzed.

4.2. Influence of Movements on Pressure Coefficients

Figure 5(a) to Figure 5(d) show the mean values of the pressure coefficients around the cylinder, as a function of the angle, for the 4 cases shown in Table 1. The graphs on the left correspond to cylinder 0 (lower cylinder) and the right graphs correspond to cylinder 1 (upper cylinder).

For case 1, Figure 5(a), the pressure distribution along the cylinder with clockwise rotation has similar behavior for the different spacing ratios. This uniformity in the behavior becomes more pronounced for L/D greater than 2.0, situation in which the vortex wake of each cylinder becomes more independent. It is verified for all the spacing ratios, that at the stagnation point, $\theta = 0^{\circ}$ (minimum velocity), the local pressure is maximum, consequently, the pressure coefficient is close to the unit value. As it runs through the cylinder from the front part ($\theta = 0^{\circ}$), to the bottom ($\theta = 90^{\circ}$) and then to the rear ($\theta = 180^{\circ}$) and top of the cylinder ($\theta = 270^{\circ}$), the mean pressure coefficient reduces up to a value of approximately—2.32, for $\theta = 273^{\circ}$. It is noted a displacement for the right, of the points corresponding to the minimum C_p, as the spacing ratio increases, going from θ equal to 262.5° ($C_p = -1.38$) to θ around 273° ($C_p = -2.32$). This behavior is coherent with the rotation direction of the cylinder.

For the cylinder with rotation-oscillation movement, the pressure distribution around the cylinder, also presents similar behavior for L/D greater than 2. This implies that, as the spacing increases, the influence of a moving cylinder on the other cylinder also in motion, decreases. For $L/D < 2$, the pressure distribution is more irregular, whereas, as the influence of spacing decreases, the pressure distribution becomes more regular, highlighting two points of lower pressure, one for $\theta = 108.75^{\circ}$ ($C_p = -2.19$) and another for $\theta = 255^{\circ}$ ($C_p = -2.45$). The lowest average pressure coefficient is verified for L/D = 1.5, being $\theta = 172.5^{\circ}$ and $C_p = -2.58$.

For case 2, Figure 5(b), in which the movement type of the upper cylinder is

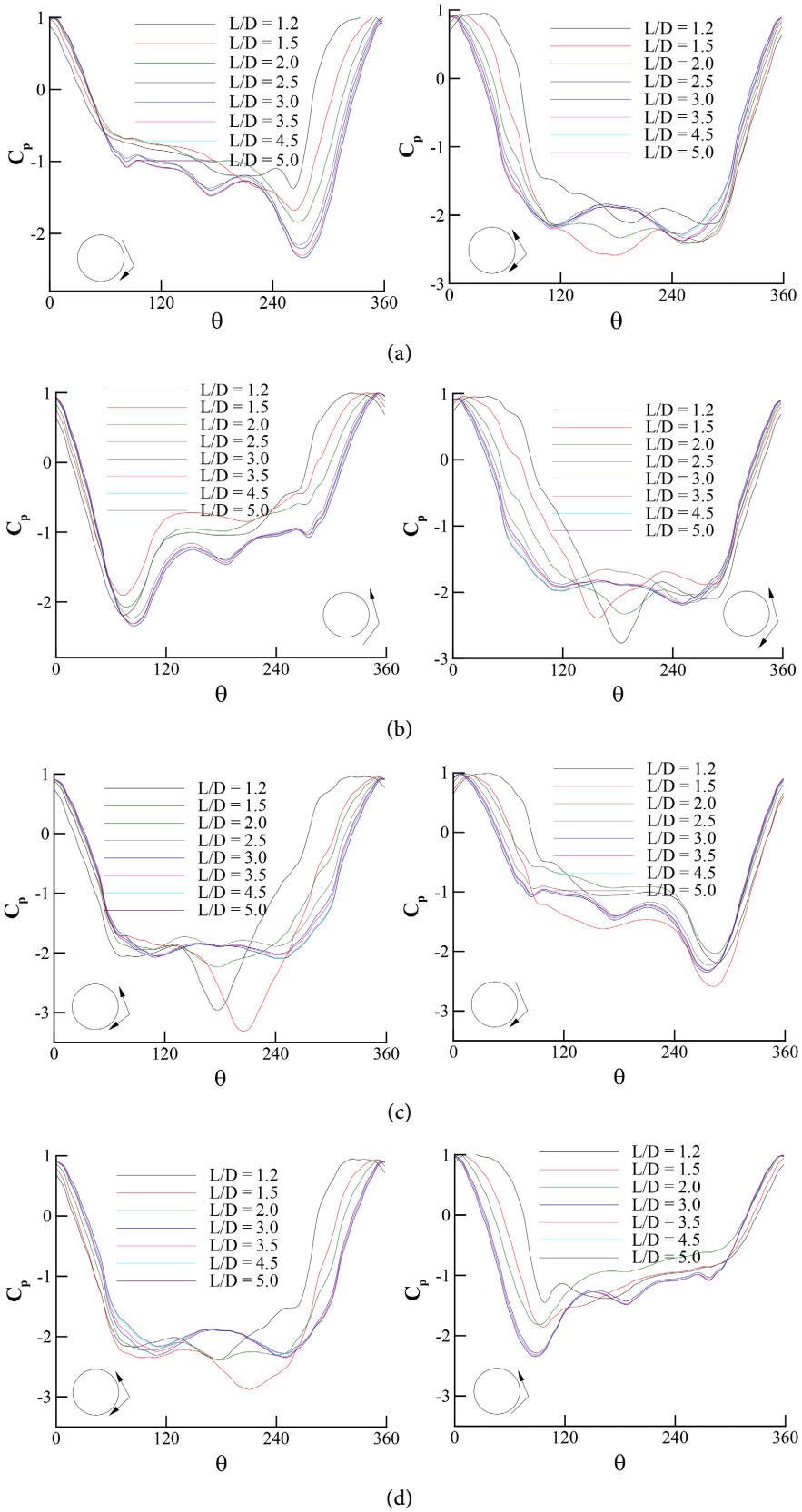

Figure 5. (a) Distribution of the mean pressure coefficient versus angle, case 1. (b) Case 2. (c) Case 3. (d) Case 4.

maintained and only the movement of the lower cylinder is changed, from clockwise to counterclockwise rotation, the pressure distribution along the cylinder presented behavior coherent with the types of movements. For the two cases analyzed so far, the minimum velocity point ($\theta = 0^\circ$) is the same, therefore, $C_p = 1.0$. Once the lower cylinder rotates counterclockwise, it is coherent that the minimum value for the average pressure coefficient ($C_p = -2.35$), corresponds to the bottom of the cylinder, $\theta = 85^\circ$, being contrary to the observed in case 1. With the increase in the spacing between the cylinders, there is oscillation in relation to the points of occurrence of low pressure values. Thus being, there is an increase in the coefficient when the spacing goes from L/D = 1.2 ($\theta = 75^\circ$ and $C_p = -2.2$) to L/D = 1.5 ($\theta = 74.85^\circ$ and $C_p = -1.92$), followed by a reduction when L/D = 2.0 ($\theta = 76.5^\circ$, $C_p = -2.1$) and L/D = 2.5 ($\theta = 82.875^\circ$ and $C_p = -2.24$). For the other spacings there are no significant oscillations.

Considering the cylinder with rotation-oscillation movement, the greatest differences in the pressure distribution around the cylinder are also verified for spacing ratios lower than 2.5. For larger spacings, the behavior tends to stabilize, due to reduction of the influence between the cylinders. The smallest mean value of the coefficient is obtained for L/D = 1.2 ($C_p = -2.76$), followed by its increase with the increase of the spacing ratio and keeping the value approximately the same for $L/D \geq 2.5$. Thus, the influence of the direction of rotation, clockwise (CR) or counterclockwise (CCR), in the pressure distribution along the cylinder with rotation-oscillation (RO) movement is confirmed.

Changing the position of the cylinder with RO motion, **Figure 5(c)** shows the pressure distribution along the cylinders surface for case 3.

It is noted that the interference between the cylinders for small spacing ratios is quite significant, so that the pressure distribution for cylinder 0 with RO is similar to that obtained for cylinder 1 with CR.

In both cylinders there is a reduction in the mean value of the pressure coefficient, with the increase in the spacing ratio from 1.2 to 1.5, of 11.5% and 18.2%, for cylinders 0 and 1, respectively. It is worth to point out that for the cylinder with RO movement, the minimum coefficient reduced from −2.96 ($\theta = 177.3^\circ$ and L/D = 1.2) to −3.3 ($\theta = 206.85^\circ$ and L/D = 1.5), while for cylinder 1 the reduction is from −2.2 ($\theta = 286.5^\circ$ and L/D = 1.2) to −2.6 ($\theta = 282.63^\circ$ and L/D = 1.5).

Figure 5(d) shows the mean pressure distribution for case 4, in which cylinder 0 maintained the RO movement, while cylinder 1 changed to CCR.

For this combination of movements, a more irregular behavior is also noted for low L/D values, keeping the characteristic behavior for larger spacings. Such irregularity is due to the greater interaction between the cylinders due to their proximity. For cylinder 0, the lowest mean pressure coefficient is obtained for L/D = 1.5 and θ = 210°, being equal to −2.88. And, for cylinder 1, the smallest average coefficient is obtained for spacing ratios greater than 2.5, whose behavior remains approximately the same, being equal to −2.31 for θ = 88.165°.

4.3. Influence of Movements on Fluid Dynamics Coefficients

Figure 6 shows the mean values of the drag coefficients for cylinders 0 and 1, considering the 4 analyzed cases. For cylinder 0 with CR (case 1), it is noted that the mean values of C_d decrease with the increase of the spacing ratio up to L/D = 2.0 and after oscillate around an average value of 1.6079 for the other spacings. In counterpart, when in CCR (case 2), the drag decreases slightly from L/D = 1.2 to 1.5 and then increases tending to the values obtained with the CR, but keeping smaller. It is thus verified, that the rotation movement has a more significant influence on drag for small spacing ratios. As the spacing increases, regardless of the rotation direction, this influence becomes practically negligible. On the other hand, cylinder 0, when in RO movement, presents mean values of C_d much higher than those obtained when in rotation movement. This implies that drag reduction can occur with greater or lesser efficiency, depending on the type of movement.

Considering cylinder 1, high drag values are also noted when in RO movement, with similar behavior to cylinder 0 with the same type of movement. It is interesting to point out that the behavior of the drag coefficient for cylinder 1 with CCR is similar to that observed for cylinder 0 with CR.

And, the behavior of cylinder 1 with CR is similar to that of cylinder 0 with CCR, showing divergence only for L/D equal to 1.5. Such behaviors lead to conclude that not only the type of movement influences the drag, as also the position of the cylinder.

In view of the above, it can be said that the rotation movement is more efficient in reducing drag than the rotation-oscillation movement, considering the frequency ratio studied (f_r = 0.5). However, the oscillating cylinder helps to reduce the drag of the rotating cylinder, depending on the direction of its movement and its position. This is confirmed when analyzing cylinders 0 and 1, both with clockwise rotation, but with opposite positions, in relation to oscillating cylinder. Note that when the cylinder is in the upper position, the drag is less than when it is in the lower position. And, analyzing cylinders 0 and 1, both with counterclockwise rotation, the drag is smaller when it is placed in the lower position in relation to the oscillating cylinder.

In counterpart, the RO cylinder, for $L/D \leq 1.5$, presented lower drag when in the upper position in relation to the cylinder with CCR. With increasing spacing ratio, the mean values of C_d are approximately the same, independently of the oscillating cylinder position relative to the rotating cylinder.

The mean values of the lift coefficient are shown in Figure 7. A similar behavior is observed in all analyzed cases. However, comparing cases 1 and 2, in which the direction of rotation is opposite, the average coefficients are positive for the clockwise rotation, with the exception of the smallest spacing ratio, and present negative values for the counterclockwise rotation, what is coherent. The same behavior is also verified for cylinder 1, cases 3 and 4.

As already commented, the cylinder position, if lower or upper, influences the

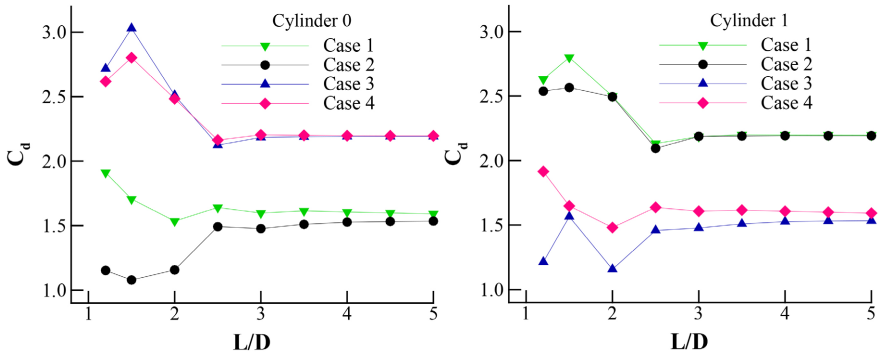

Figure 6. Mean values of drag coefficients as a function of *L*/*D*.

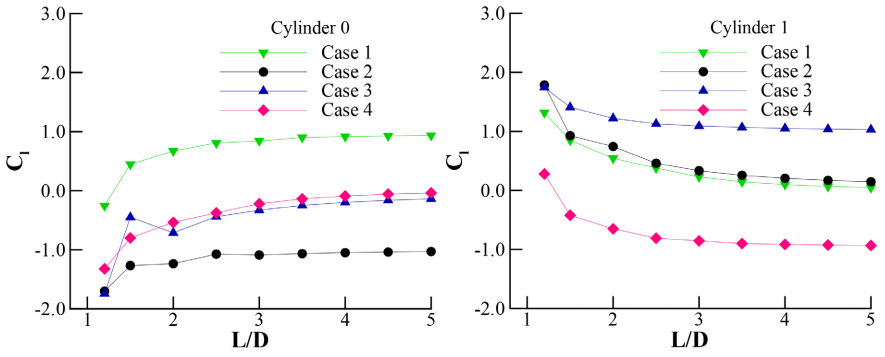

Figure 7. Mean values of the lift coefficients as a function of *L*/*D*.

behavior of the fluid dynamics coefficients. For small spacing ratios, the average values of the lift coefficient increase tending to a more constant value, when the cylinder is in the lower position, and presents opposite behavior when in the upper position.

In this way, the greatest influence of one cylinder over the other is verified for small spacings. As the spacing increases, this influence decreases. This is due to the fact that the vortices wakes become more and more independent. It is also interesting to point out, that the cylinder with rotation-oscillation movement, when in the upper position (cylinder 1), which correspond to cases 1 and 2, present positive mean coefficients for all spacing ratios. On the other hand, considering the same type of movement, but with the cylinder in the lower position (cylinder 0), which refer to cases 3 and 4, the average values of the lift coefficient are negative. Such behaviors are due to the influence of the rotating cylinder. Depending on the combination of movements, as well as the positions of the cylinders, the sign of the lift coefficient of the oscillating cylinder may or may not be the same as that of the rotating cylinder. The obtained results show that the combination of RO (cylinder 1) with CCR (cylinder 0) and, the combination of RO (cylinder 0) with the CR (cylinder 1), results mean lift coefficients of opposite signs to those of the respective rotating cylinders. On the other hand, combining RO (cylinder 1) with CR (cylinder 0) and, RO (cylinder 0) with CCR (cylinder 1), results in coefficients of the same signs to those of the respective rotating cylinders.

It is still verified, that the mean lift coefficients (C_ℓ) of the oscillating cylinder, when in the upper position in relation to the rotating cylinder (cases 1 and 2), decrease with the increase of the spacing ratio. On the other hand, when in the lower position (case 4), the values of C_ℓ increase with increasing spacing and, considering case 3, the values oscillate to $L/D \leq 2.0$ and then increase with spacing. Already the cylinder with clockwise rotation, when in the lower position (case 1), the values of C_ℓ increase with the increase of L/D and decrease when in the upper position (case 3). And, the cylinder with the counterclockwise rotation, presents a decrease of C_ℓ with the increase of L/D for case 4 and, for case 2, the values oscillate for L/D equal to 2.5 and 3.0 and then increase. Finally, it is concluded that case 3 is the combination that resulted greater lift.

5. Conclusions

In this work, the IB methodology is used to simulate flow around two moving circular cylinders, arranged side by side, for Re = 1000, $A = 3$, $a = 0.5$, $f_r = 0.5$ and different L/D. The most important conclusions of the numerical simulations are summarized as follow:

1) For small spacing ratios, the two cylinders behave as a single bluff body, regardless of movement type. This is proven by the 2S vortex shedding pattern. However, it is important to point out that the alternation in the combination of movements influences the longitudinal and transverse spacing of the vortices and the time in which the vortices are generated and released from the cylinders.

2) The alternating motions (Table 1) have more significant effect on the pressure distribution around the cylinder surface when they are closer to each other. With distancing between them, the pressure distribution acquires the characteristic behavior of each movement. The lowest average pressure coefficient ($C_p = -3.3$) is obtained for the oscillating cylinder placed side by side with the clockwise rotation cylinder, case 3 and $L/D = 1.5$.

3) The rotation influences the drag more significantly for small spacing ratios, being practically negligible such influence as the spacing increases. Furthermore, the rotating cylinder when in the lower position, is more effective in reducing drag when rotating counterclockwise than clockwise. On the other hand, when located in the upper position, the drag reduction is greater when it rotates clockwise, due to the fact that the shear layers coming from the cylinder going toward those originated by the oscillating cylinder.

4) The oscillating cylinder, may presents average lift coefficient, positive or negative, depending on its position relative to the rotating cylinder.

5) The lowest lift coefficients values are obtained for the cylinder with CCR (case 2).

Another work is being done, in which the influence of motion and the position of one cylinder relative to the other is being investigated through the velocity and pressure fields and the power spectrum of the lift coefficient signal. In addition, different frequency ratios will also be analyzed. As future perspectives

can be mentioned:

- Simulate cases of fluid-structure interaction, increasing the free stream velocity with oscillating cylinder and also the same analysis with decreasing velocity;
- Perform three-dimensional simulations;
- Simulate other types of flows, such as confined and non-isothermal flows, among others.

Acknowledgements

The author thanks the Faculty of Civil Engineering of the Federal University of Uberlândia for the given support.

Conflicts of Interest

The author declares no conflicts of interest regarding the publication of this paper.

References

[1] Aguedal, L., Semmar, D., Berrouk, A.S., Azzi, A. and Oualli, H. (2018) 3D Vortex Structure Investigation Using Large Eddy Simulation of Flow around a Rotary Oscillating Circular Cylinder. *European Journal of Mechanics/BFluids*, **71**, 113-125. https://doi.org/10.1016/j.euromechflu.2018.04.001

[2] Nobari, M.R.H. and Ghazanfarian, J. (2009) A Numerical Investigation of Fluid Flow over a Rotating Cylinder with Cross Flow Oscillation. *Computers & Fluids*, **38**, 2026-2036. https://doi.org/10.1016/j.compfluid.2009.06.008

[3] Mittal, H.V.R. and Al-Mdallal, Q.M. (2018) A Numerical Study of Forced Convection from an Isothermal Cylinder Performing Rotational Oscillations in a Uniform Stream. *International Journal of Heat and Mass Transfer*, **127**, 357-374. https://doi.org/10.1016/j.ijheatmasstransfer.2018.07.022

[4] Da Silva, A.R. and de Lima, A.M.G. (2020) Analysis of Flow Dynamics around Two Rotating Circular Cylinders in Tandem and Side by Side. *International Journal of Advanced Engineering Research and Science* (*IJAERS*), **7**, 366-379. https://doi.org/10.22161/ijaers.76.45

[5] Da Silva, A.R., Silveira-Neto, A. and de Lima, A.M.G. (2015) Rotational Oscillation Effect on Flow Characteristics of a Circular Cylinder at Low Reynolds Number. *World Journal of Mechanics*, **5**, 195-209. https://doi.org/10.4236/wjm.2015.510019

[6] Da Silva, A.R., Silveira-Neto, A. and de Lima, A.M.G. (2016) Flow-Induced Vibration of a Circular Cylinder in Cross-Flow at Moderate Reynolds Number. *Journal of the Brazilian Society of Mechanical Sciences and Engineering*, **38**, 1185-1197. https://doi.org/10.1007/s40430-015-0314-8

[7] Hu, X., Zhang, X. and You, Y. (2019) On the Flow around Two Circular Cylinders in Tandem Arrangement at High Reynolds Numbers. *Ocean Engineering*, **189**, Article ID: 106301. https://doi.org/10.1016/j.oceaneng.2019.106301

[8] Cimarelli, A., Leonforte, A. and Angeli, D. (2018) Direct Numerical Simulation of the Flow around a Rectangular Cylinder at a Moderately High Reynolds Number. *Journal of Wind Engineering & Industrial Aerodynamics*, **174**, 39-49. https://doi.org/10.1016/j.jweia.2017.12.020

[9] Vicente-Ludlam, D., Barrero-Gil, A. and Velazquez, A. (2017) Flow-Induced Vibration of a Rotating Circular Cylinder Using Position and Velocity Feedback. *Journal of Fluids and Structures*, **72**, 127-151. https://doi.org/10.1016/j.jfluidstructs.2017.05.001

[10] Vijay, K., Srinil, N., Zhu, H., Bao, Y., Zhou, D. and Han, Z. (2020) Flow-Induced Transverse Vibration of an Elliptical Cylinder with Different Aspect Ratios. *Ocean Engineering*, **214**, Article ID: 107831. https://doi.org/10.1016/j.oceaneng.2020.107831

[11] Narváez, G.F., Schettini, E.B. and Silvestrini, J.H. (2020) Numerical Simulation of Flow-Induced Vibration of Two Cylinders Elastically Mounted in Tandem by Immersed Moving Boundary Method. *Applied Mathematical Modelling*, **77**, 1331-1347. https://doi.org/10.1016/j.apm.2019.09.007

[12] Chen, W., Ji, C. and Xu, D. (2019) Vortex-Induced Vibrations of Two Side-by-Side Circular Cylinders with Two Degrees of Freedom in Laminar Cross-Flow. *Computers and Fluids*, **193**, Article ID: 104288. https://doi.org/10.1016/j.compfluid.2019.104288

[13] Wu, Y.L. (2017) Numerical Simulation of Flows Past Multiple Cylinders Using the hybrid Local Domain Free Discretization and Immersed Boundary Method. *Ocean Engineering*, **141**, 477-492. https://doi.org/10.1016/j.oceaneng.2017.06.045

[14] Chehreh, B.B. and Javadi, K. (2018) Flow Control around a Circular Cylinder with Swinging Thin Plates. *Journal of Fluids and Structures*, **81**, 738-760. https://doi.org/10.1016/j.jfluidstructs.2018.06.010

[15] Zheng, H. and Wang, J. (2017) Numerical Study of Galloping Oscillation of a Two-Dimensional Circular Cylinder Attached with Fixed Fairing Device. *Ocean Engineering*, **130**, 274-283. https://doi.org/10.1016/j.oceaneng.2016.11.074

[16] Ping, H., Zhu, H., Zhang, K., Wang, R., Zhou, D., Bao, Y. and Han, Z. (2020) Wake Dynamics behind a Rotary Oscillating Cylinder Analyzed with Proper Orthogonal Decomposition. *Ocean Engineering*, **218**, Article ID: 108185. https://doi.org/10.1016/j.oceaneng.2020.108185

[17] Peskin, C.S. (1977) Numerical Analysis of Blood Flow in the Heart. *Journal of Computational Physics*, **25**, 220-252. https://doi.org/10.1016/0021-9991(77)90100-0

[18] Chen, Y., Djidjeli, K. and Xie, Z-T. (2020) Large Eddy Simulation of Flow Past Stationary and Oscillating Square Cylinders. *Journal of Fluids and Structures*, **97**, Article ID: 103107. https://doi.org/10.1016/j.jfluidstructs.2020.103107

[19] Khalili, M.E., Larsson, M. and Müller, B. (2018) Immersed Boundary Method for Viscous Compressible Flows around Moving Bodies. *Computers and Fluids*, **170**, 77-92. https://doi.org/10.1016/j.compfluid.2018.04.033

[20] Lo, D.C., Lee, C.-P. and Lin, I.-F. (2018) An Efficient Immersed Boundary Method for Fluid Flow Simulations with Moving Boundaries. *Applied Mathematics and Computation*, **328**, 312-337. https://doi.org/10.1016/j.amc.2018.01.022

[21] Peskin, C.S. and McQueen, D.M. (1995) A General Method for the Computer Simulation of Biological Systems Interacting with Fluids. *SEB Symposium on Biological Fluid Dynamics*, **49**, 265-276.

[22] Lima E Silva, A.L.F., Silveira-Neto, A. and Damasceno, J.J.R. (2003) Numerical Simulation of Two-Dimensional Flows over a Circular Cylinder Using the Immersed Boundary Method. *Journal of Computational Physics*, **189**, 351-370. https://doi.org/10.1016/S0021-9991(03)00214-6

[23] Chorin, A. (1968) Numerical Solution of the Navier-Stokes Equations. *Mathematics*

of Computations, **22**, 745-762. https://doi.org/10.1090/S0025-5718-1968-0242392-2

[24] Schneider, G.E. and Zedan, M. (2007) A Modified Strongly Implicit Procedure for the Numerical Solution of Field Problems. *Numerical Heat Transfer*, **4**, 1-19. https://doi.org/10.1080/01495728108961775

[25] Pope, S.B. (2005) Turbulent Flows. Cambridge University Press, Cambridge, MA.

[26] Reynolds, O. (1895) On the Dynamical Theory of Incompressible Viscous Fluids and the Determination of the Criterion. *Philosophical Transactions of the Royal Society of London*, **186**, 123-164. https://doi.org/10.1098/rsta.1895.0004

[27] Smagorinsky, J. (1963) General Circulation Experiments with Primitive Equations, *Monthly Weather Review*, **91**, 99-164. https://doi.org/10.1175/1520-0493(1963)091<0099:GCEWTP>2.3.CO;2

[28] He, J.-W., Glowinski, R., Metcalfe, R., Nordlander, A. and Periaux, J. (2000) Active Control and Drag Optimization for Flow Past a Circular Cylinder: I. Oscillatory Cylinder Rotation. *Journal of Computational Physics*, **163**, 83-117. https://doi.org/10.1006/jcph.2000.6556

[29] Williamson, C.H.K. and Jauvtis, N. (2004) A High-Amplitude 2T Mode of Vortex-Induced Vibration for a Light Body in XY Motion. *European Journal of Mechanics-B/Fluids*, **23**, 107-114. https://doi.org/10.1016/j.euromechflu.2003.09.008